Weak ferromagnetism and spiral spin structures in honeycomb Hubbard planes

M A N Araújo[1,2] and N M R Peres[2,3]

[1]Departamento de Física, Universidade de Évora, P-7000-671, Évora, Portugal
[2]Center of Physics, Universidade do Minho, P-4710-057, Braga, Portugal
[3]Department of Physics, Boston University, 590 Commonwealth Avenue, Boston, MA 02215,USA

E-mail: mana@uevora.pt

Abstract. Within the Hartree Fock- RPA analysis, we derive the spin wave spectrum for the weak ferromagnetic phase of the Hubbard model on the honeycomb lattice. Assuming a uniform magnetization, the polar (optical) and acoustic branches of the spin wave excitations are determined. The bipartite lattice geometry produces a $\boldsymbol{q}$-dependent phase difference between the spin wave amplitudes on the two sub-lattices. We also find an instability of the uniform weakly magnetized configuration to a weak antiferromagnetic spiraling spin structure, in the lattice plane, with wave vector $\boldsymbol{Q}$ along the $\Gamma - K$ direction, for electron densities $n > 0.6$. We discuss the effect of diagonal disorder on both the creation of electron bound states, enhancement of the density of states, and the possible relevance of these effects to disorder induced ferromagnetism, as observed in proton irradiated graphite.

PACS numbers: 71.10.Fd, 75.10.Lp, 75.30.Ds, 75.30.Kz, 81.05.Uw

Submitted to: *J. Phys.: Condens. Matter*

1. Introduction

Recent interest in strongly correlated systems in non-square lattices, such as the triangular, honeycomb and kagomé lattices, is justified by the possible realization of exotic metallic [1, 2], magnetic [3, 4] and superconducting states [5] both in inorganic and organic materials. From the organic side, graphite and related carbon allotropes are physical systems where growing evidence for exotic types of ground states is being accumulated during the last few years. In graphite, for example, experimental research put forward evidence for unusual metallic and magnetic properties [2, 6, 7, 4]. In particular, ferromagnetism has been observed at high temperature in graphite [6] which may not be due to magnetic impurities. Also, the observation [2] of magnetic order induced by proton irradiation challenges the theoretical description. Graphite is not alone on the ferromagnetic-order-by-disorder scenario, with the inorganic $CaRuO_3$ material also exhibiting disorder-induced ferromagnetism [8]. Recent experimental work [9, 10, 11] has produced atomic thin graphite planes where the exciting physics of 2D Dirac fermions may be directly observable. Motivated by these experimental studies and because the microscopic origin of ferromagnetism in these compounds is far from being understood, we decided to study the magnetic properties of a doped Hubbard model on an honeycomb lattice – a single graphite plane. To the best of our knowledge, ferromagnetic spin waves in the honeycomb lattice (as an itinerant electron system) have not been studied in the past. The fact that the honeycomb lattice is a Bravais lattice with a basis immediately presents us the possibility of observing both polar and acoustic spin waves [12, 13]. We focus our research on the stability of the weak homogeneous ferromagnetic phase found in [14]. The paper is organized as follows: the model is introduced in section 2 and the energy spectrum for the weak homogeneous ferromagnetic system is derived; Section 3 is devoted to the description of spin waves in the weak homogeneous ferromagnetic phase; the possibility of spiral spin states is investigated in Section 4, where a spiral arrangement is found with lower energy than that of a uniform magnetization; Section 5 gives a discussion on the possibility of formation of electronic bound states, due to impurities, and of the possible relevance of disorder to experiments on proton irradiated graphite.

2. Model Hamiltonian

The Hubbard model is defined as

$$H = -\sum_{i,j,\sigma}(t_{i,j}+\mu\delta_{ij})c^{\dagger}_{i,\sigma}c_{j,\sigma} + U\sum_{i} c^{\dagger}_{i,\uparrow}c_{i,\uparrow}c^{\dagger}_{i,\downarrow}c_{i,\downarrow}\,, \tag{1}$$

where $c^{\dagger}_{i,\sigma}$ ($c_{i,\sigma}$) represents a creation (destruction) electron operator with spin σ at site i, $t_{i,j}$ is the hopping integral between two sites i and j, U is the on-site Coulomb repulsion, and μ is the chemical potential. In the honeycomb lattice we identify two sub-lattices, A and B (see figure 1), where the primitive vectors of the underlying triangular lattice are denoted by $\boldsymbol{a}_1$ and $\boldsymbol{a}_2$. For later use we also define the vector $\boldsymbol{a}_3 \equiv (\boldsymbol{a}_1 - \boldsymbol{a}_2)$. The

reciprocal lattice vectors are $\boldsymbol{b}_1$ and $\boldsymbol{b}_2$ and define a hexagonal shaped first Brillouin Zone. Also shown in figure 1 are the vectors connecting any A atom to its nearest neighbours, denoted as $\boldsymbol{\delta}_1$, $\boldsymbol{\delta}_2$ and $\boldsymbol{\delta}_3$. The electrons leaving on each sub-lattice will be

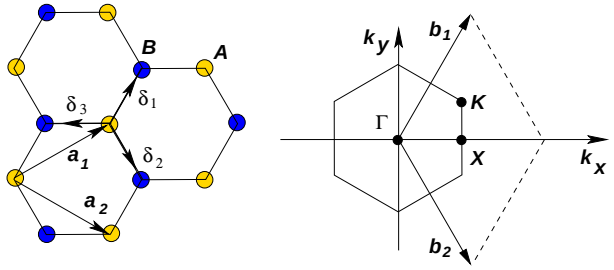

Figure 1. Primitive vectors ($\boldsymbol{a}_1$ and $\boldsymbol{a}_2$) for the honeycomb lattice. The vectors $\boldsymbol{\delta}_1$, $\boldsymbol{\delta}_2$ and $\boldsymbol{\delta}_3$ connect the A site to its three neighbouring B sites. The hexagonal first Brillouin zone corresponds to the reciprocal lattice vectors, $\boldsymbol{b}_1$ and $\boldsymbol{b}_2$.

denoted by field operators a and b, respectively. The Fourier transformation between real and momentum spaces is given by:

$$a^\dagger_{i,\sigma} = \frac{1}{\sqrt{N_A}} \sum_{\boldsymbol{k}} e^{i\boldsymbol{k}\cdot\boldsymbol{R}_i} a^\dagger_{\boldsymbol{k},\sigma}\,, \quad b^\dagger_{i,\sigma} = \frac{1}{\sqrt{N_B}} \sum_{\boldsymbol{k}} e^{i\boldsymbol{k}\cdot\boldsymbol{R}_i} b^\dagger_{\boldsymbol{k},\sigma}\,, \tag{2}$$

and we take $N_A = N_B = N$ as the number of unit cells. In the calculations below, we shall consider first and second neighbour hopping integrals, t and t', respectively. The Hubbard model then takes the form:

$$\begin{aligned} H = & \sum_{\boldsymbol{k},\sigma} (D(\boldsymbol{k}) - \mu)(a^\dagger_{\boldsymbol{k},\sigma} a_{\boldsymbol{k},\sigma} + b^\dagger_{\boldsymbol{k},\sigma} b_{\boldsymbol{k},\sigma}) \\ & + \sum_{\boldsymbol{k},\sigma} [\phi(\boldsymbol{k}) a^\dagger_{\boldsymbol{k},\sigma} b_{\boldsymbol{k},\sigma} + \phi^*(\boldsymbol{k}) b^\dagger_{\boldsymbol{k},\sigma} a_{\boldsymbol{k},\sigma}] + H_U\,, \end{aligned} \tag{3}$$

with

$$\begin{aligned} D(\boldsymbol{k}) &= -2t' \sum_{i=1}^{3} \cos(\boldsymbol{a}_i \cdot \mathbf{k})\,, \\ \phi(\boldsymbol{k}) &= -t \sum_{i=1}^{3} e^{i\boldsymbol{k}\cdot\boldsymbol{\delta}_i}\,. \end{aligned} \tag{4}$$

In the ferromagnetic ground state, the average occupancy of lattices sites is given by

$$\langle a^\dagger_{i,\sigma} a_{i,\sigma} \rangle = \frac{n}{2} + \sigma \frac{m}{2}\,, \quad \langle b^\dagger_{i,\sigma} b_{i,\sigma} \rangle = \frac{n}{2} + \sigma \frac{m}{2}\,, \tag{5}$$

with the spin index $\sigma = \pm 1$. This may also be generalized to describe antiferromagnetic ordering if we replace m with $-m$ in one of the equations (5) [14]. An Hartree-Fock treatment of the Hubbard term, H_U, taking into account equation (5), yields a set of quasi-particle bands given by

$$E^\alpha_\sigma(\boldsymbol{k}) = D(\boldsymbol{k}) + \frac{U}{2}(n - \sigma m) + \alpha |\phi_{\boldsymbol{k}}|\,, \tag{6}$$

where $\alpha = \pm$ is a band index. In the ferromagnetic phase the single particle Green's functions can be written, in momentum space, as:

$$\mathcal{G}_\sigma^{aa}(i\omega_n, \boldsymbol{k}) = \sum_{j=\pm} \frac{1/2}{i\omega_n - E_\sigma^j(\boldsymbol{k})} \tag{7}$$

$$\mathcal{G}_\sigma^{ab}(i\omega_n, \boldsymbol{k}) = \sum_{j=\pm} \frac{j e^{i\delta(\boldsymbol{k})}/2}{i\omega_n - E_\sigma^j(\boldsymbol{k})} \tag{8}$$

$$\mathcal{G}_\sigma^{ba}(i\omega_n, \boldsymbol{k}) = \sum_{j=\pm} \frac{j e^{-i\delta(\boldsymbol{k})}/2}{i\omega_n - E_\sigma^j(\boldsymbol{k})} \tag{9}$$

$$\mathcal{G}_\sigma^{bb}(i\omega_n, \boldsymbol{k}) = \mathcal{G}_\sigma^{aa}(\omega_n, \boldsymbol{k}), \tag{10}$$

where we have defined $e^{i\delta(\boldsymbol{k})} = \phi(\boldsymbol{k})/|\phi(\boldsymbol{k})|$. The Hartree-Fock magnetization is given by $m = (1/2N)\sum_{\boldsymbol{k},\alpha,\sigma} \sigma f[E_\sigma^\alpha(\boldsymbol{k})]$.

Since we are mainly concerned with the ferromagnetic phase, the calculations in sections 3 and 4 are performed for an electronic density smaller than half filling. Therefore, electrons at the Fermi level will not be treated as massless Dirac fermions. Such treatment is usually appropriate for electrons in graphite planes at half filling (or close to half filling) [15].

3. Magnetic collective excitations

We obtain the magnetic collective excitations from the poles of the transverse spin susceptibility calculated in the RPA approximation. Because there are two sub-lattices, the susceptibility is actually a second order tensor given by the expression

$$\chi_{+-}^{i,j}(\boldsymbol{q}, i\omega_n) = \int_0^{1/T} d\tau e^{i\omega_n \tau} \langle T_\tau S_i^+(\boldsymbol{q}, \tau) S_j^-(-\boldsymbol{q}, 0)\rangle \tag{11}$$

where $i, j = a, b$ are sub-lattice labels and $S_i^+(\boldsymbol{q})$, $S_j^-(\boldsymbol{q})$ are the spin-raising and lowering operators for each sub-lattice. The RPA expansion gives a Dyson equation for the transverse spin susceptibility, which can by written, in matrix form, as

$$\boldsymbol{\chi}(\boldsymbol{q}, i\omega_n) = \Big[\mathbf{1} - \frac{U}{N}\boldsymbol{\chi}^0(\boldsymbol{q}, i\omega_n)\Big]^{-1} \boldsymbol{\chi}^0(\boldsymbol{q}, i\omega_n) \tag{12}$$

where $\mathbf{1}$ denotes the 2×2 identity matrix. The poles of the susceptibility tensor, corresponding to the magnetic excitations, are then obtained from the condition:

$$\det\Big[\mathbf{1} - \frac{U}{N}\boldsymbol{\chi}^0(\boldsymbol{q}, \omega + i0^+)\Big] = 0. \tag{13}$$

Below the particle-hole continuum of excitations, the spectral (delta-function contributions) part in $\chi_{+-}^{(0)ij}(\boldsymbol{q}, \omega + i0^+)$ vanish and there is the additional relation $\chi_{+-}^{(0)ba} = (\chi_{+-}^{(0)ab})^*$. The zero order susceptibility tensor, $\boldsymbol{\chi}_{+-}^{(0)}(\boldsymbol{q}, \omega)$, can be written as

$$\boldsymbol{\chi}_{+-}^{(0)}(\boldsymbol{q}, i\omega_n) = -\frac{1}{4} \sum_{\boldsymbol{k};\alpha_1,\alpha_2=\pm} \frac{f_\uparrow^{\alpha_1}(\boldsymbol{k}) - f_\downarrow^{\alpha_2}(\boldsymbol{k}-\boldsymbol{q})}{i\omega_n + E_\uparrow^{\alpha_1}(\boldsymbol{k}) - E_\downarrow^{\alpha_2}(\boldsymbol{k}-\boldsymbol{q})} \mathcal{A}(\boldsymbol{k}, \boldsymbol{q}) \tag{14}$$

where the matrix $\mathcal{A}(\boldsymbol{k}, \boldsymbol{q})$ contains the coherence factors:

$$\mathcal{A}(\boldsymbol{k}, \boldsymbol{q}) = \begin{pmatrix} 1 & \beta(\boldsymbol{k}, \boldsymbol{q}) \\ \beta^*(\boldsymbol{k}, \boldsymbol{q}) & 1 \end{pmatrix}, \tag{15}$$

$\beta(\boldsymbol{k},\boldsymbol{q}) = \exp[-i\delta(\boldsymbol{k}) + i\delta(\boldsymbol{k}-\boldsymbol{q})]$, with $f_{\downarrow}^{\alpha_2}(\boldsymbol{k})$ representing the Fermi function with argument $E_{\downarrow}^{\alpha_2}(\boldsymbol{k})$, and equivalent representations hold for the other cases.

In addition to the collective ferromagnetic spin waves there are also single particle flip-spin excitations which define the so called Stoner continuum. In our case we may have up to four regions in the energy-momentum plane associated with the latter type of excitations. Their spectra are given by

$$\Delta^{\alpha_1,\alpha_2}(\boldsymbol{q}) = E_{\downarrow}^{\alpha_1}(\boldsymbol{k}-\boldsymbol{q}) - E_{\uparrow}^{\alpha_2}(\boldsymbol{k})\,. \tag{16}$$

Depending on the position of the Fermi level, one or two of the regions defined by equation (16) may not occur because the bands may be empty. Because we have the lower (E_{σ}^{-}) bands partially filled, there always are two Stoner regions given by $\Delta^{-,-}(\boldsymbol{q})$ and $\Delta^{+,-}(\boldsymbol{q})$. We consider only this case below (for the other cases the results are qualitatively the same). In figures 2 and 3 the left panel shows the the Stoner continuum defined by $\Delta^{-,-}(\boldsymbol{q})$ as the area enclosed by the dashed-dotted line starting at $\Delta^{-,-}(0) = Um$. The model parameters have been chosen so that the system is definitely not antiferromagnetic. In figures 2 and 3 we plot the solutions to equation (13). It is clear that the system has two different types of collective magnetic excitations, namely the usual acoustic mode $\omega_{ac}(\boldsymbol{k})$ and the polar or optical mode $\omega_{opt}(\boldsymbol{k})$, associated with the existence of two atoms per unit cell [12, 13]. It is quite interesting that the behaviour of both branches of excitations does not follow the same trend along different directions of the Brillouin zone: along the $\Gamma - X$ direction (see figure 2), for example, and for $|\boldsymbol{q}| > 0.25\Gamma X$ only the optical branch remains. On the other hand, in the $\Gamma - K$ direction (see figure 3) it is the optical branch that vanishes at $|\boldsymbol{q}| \approx 0.2\Gamma K$ while the acoustic mode survives. The vanishing frequency of the acoustic (or optical) modes at finite momentum is associated with an instability of the homogeneous weak ferromagnetic phase toward a state exhibiting possibly weak ferromagnetic order in the z direction and spiral order in the xy plane, which will be analyzed in section 4 below.

The eigenvector of the matrix $\boldsymbol{\chi}^{(0)}(\boldsymbol{q},\,\omega(\boldsymbol{q}))$ that is associated with the eigenvalue N/U gives the spin wave amplitudes over the A and B sub-lattices. We note that equation (13) is equivalent to the eigenproblem

$$\frac{1}{N}\boldsymbol{\chi}^{0}(\boldsymbol{q},\omega+i0^{+})\begin{bmatrix}\langle S_A^{+}\rangle\\ \langle S_B^{+}\rangle\end{bmatrix} = \frac{1}{U}\begin{bmatrix}\langle S_A^{+}\rangle\\ \langle S_B^{+}\rangle\end{bmatrix}, \tag{17}$$

where $\langle S_A^{+}\rangle, \langle S_B^{+}\rangle$ denote the spin wave amplitudes over the two sub-lattices [16]. In our case, $\chi^{(0),aa} = \chi^{(0),bb}$ and $\chi^{(0)ab} = (\chi^{(0)ba})^{*}$. The equations for the eigenvalue λ and the corresponding eigenvector are:

$$\lambda \quad = \chi^{(0),aa} \pm |\chi^{(0)ab}| \tag{18}$$

$$\langle S_A^{+}\rangle = \pm\frac{\chi^{(0)ab}}{|\chi^{(0)ab}|}\langle S_B^{+}\rangle\,, \tag{19}$$

where $\lambda = N/U$ is the relevant eigenvalue, as can be seen from equation (17). Equation (19) shows that the spin wave amplitudes are related by a phase factor. Therefore, the phase of the complex matrix element $\chi^{(0)ab}$ determines the angle between the transverse

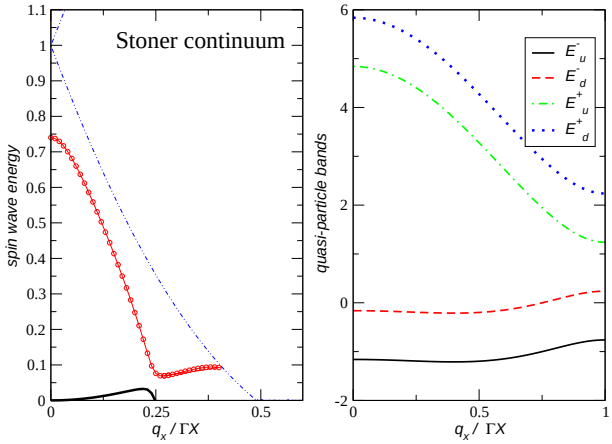

Figure 2. Left panel: Spin waves (line with circles for ω_{opt} and continuous line for ω_{ac}) and Stoner continuum border (thin dashed-dotted line) along the $\Gamma - X$ direction of the Brillouin zone. Right: band energies along the $\Gamma - X$ direction (the band energies are measured relatively to the chemical potential); The parameters are: $U = 4$, $t = 1$, $t' = -0.2$, $n = 0.75$, and the magnetization and chemical potential are $m = 0.25$ and $\mu = 0.36$. The energy through all this paper is in units of t. (Subscripts u and d in the right

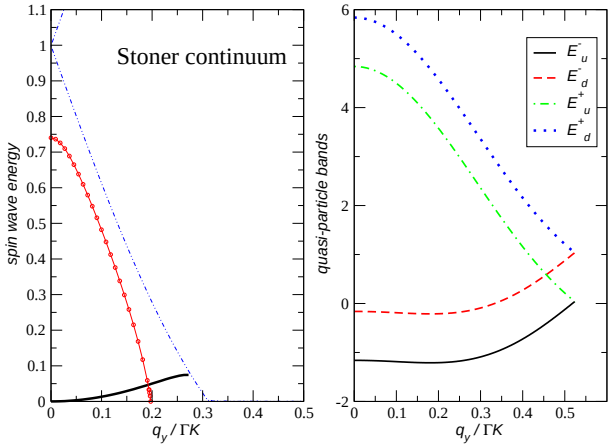

Figure 3. Left panel: Spin waves (line with circles for ω_{opt} and continuous line for ω_{ac}) and Stoner continuum border (thin dashed-dotted line) along the $\Gamma - K$ direction of the Brillouin zone. Right panel: quasi-particle band structure along the $\Gamma - K$ direction (band energies measured relative to chemical potential); The parameters are the same as in figure 2. (Subscripts u and d in the right panel denote spin projections $\uparrow$ and $\downarrow$, respectively.)

spin components $\langle S^+_A \rangle$ and $\langle S^+_B \rangle$. The optical mode in the $\Gamma - X$ direction (shown in figure 2) starts off with $\langle S^+_A \rangle = -\langle S^+_B \rangle$ for small $\boldsymbol{q}$, as expected of an optical mode, but the angle between $\langle S^+_A \rangle$ and $\langle S^+_B \rangle$ monotonically decreases from π, upon increasing wave vector, and equals $\pi/2$ when ω_{opt} attains its minimum. At that point, $\chi^{(0)ab}$ is pure imaginary. On the other hand, in the acoustic mode the angle increases from zero

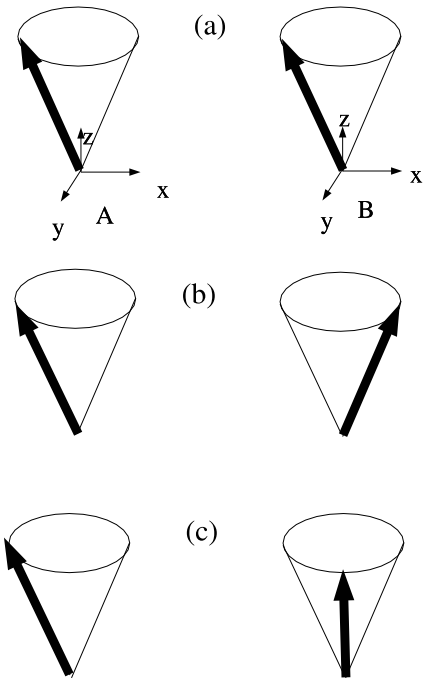

Figure 4. Relative position of the precessing spins on neighbouring A and B sites for a spin wave in the $\Gamma - X$ direction: (a) acoustic mode with small $\boldsymbol{q}$; (b) optical mode with small $\boldsymbol{q}$; (c) minimum (maximum) frequency of the optical (acoustic) mode.

to $\pi/2$, when ω_{ac} is maximum (the angle between the spins is illustrated in figure 4). As the wave vector further increases, the acoustic mode frequency rapidly decreases and vanishes at $\boldsymbol{q} \approx 0.25\boldsymbol{\Gamma X}$.

Considering now the spin waves in the $\Gamma - K$ direction, the angle between the precessing spins is always zero or π in the acoustic and optical modes, respectively. The optical mode frequency vanishes shortly after the interception with the acoustic branch and only the latter survives for increasing $\boldsymbol{q}$.

The phase difference between spin wave amplitudes just described for the $\Gamma - X$ direction is a manifestation of the complex coherence factors appearing in the single particle Green functions (8) and (9), resulting from the honeycomb lattice geometry.

4. Spiral spin states

The disappearance of the acoustic mode, at wave vector $\boldsymbol{q} \approx 0.25\boldsymbol{\Gamma X}$, and of the optical mode, at wave vector $\boldsymbol{q} \approx 0.20\boldsymbol{\Gamma K}$, suggests an instability to a spiral spin state [17]. In such a state, the spiral spin configuration is characterized by non-zero transverse magnetization at site j, $\langle S_j^+ \rangle = \langle S^+ \rangle e^{i\boldsymbol{Q}\cdot\boldsymbol{R}_j}$, in addition to a uniform alignment in the z direction, $\langle S^z \rangle$. The amplitudes of the spiral, $\langle S_{A(B)}^+ \rangle$, at sub-lattices A and B are given

by:

$$\langle S_A^+ \rangle = \frac{1}{N_c} \sum_{\boldsymbol{k}} \langle a^\dagger_{\boldsymbol{k},\uparrow} a_{\boldsymbol{k}+\boldsymbol{Q},\downarrow} \rangle$$
$$\langle S_B^+ \rangle = \frac{1}{N_c} \sum_{\boldsymbol{k}} \langle b^\dagger_{\boldsymbol{k},\uparrow} b_{\boldsymbol{k}+\boldsymbol{Q},\downarrow} \rangle. \tag{20}$$

In general, there will be a nonzero angle θ between the transverse sub-lattice magnetizations $\langle S_A^+ \rangle$ and $\langle S_B^+ \rangle$, so that $\langle S_B^+ \rangle = e^{i\theta} \langle S_A^+ \rangle$.

Following [17], the mean field equations are obtained from the minimization of the ground state energy with respect to the order parameters $\langle S^+_{A(B)} \rangle$ and $\langle S^z \rangle$. Each Bloch $\boldsymbol{k}$-state, $\gamma_{\boldsymbol{k}}$, representing an elementary excitation, is a linear superposition of the fields $a_{\boldsymbol{k},\uparrow}, a_{\boldsymbol{k}+\boldsymbol{Q},\downarrow}, b_{\boldsymbol{k},\uparrow}$ and $b_{\boldsymbol{k}+\boldsymbol{Q},\downarrow}$. Conversely, we can rewrite each of the fields as a combination of Bloch states, and recast the expectation value of the kinetic term in (3) as well as the order parameters (20) in terms of $\gamma_{\boldsymbol{k}}$ operators. Using Wick's theorem, the expectation value of the Hubbard term in the Hamiltonian (3) can be expressed as:

$$\langle H_U \rangle = U\Big(\frac{n^2}{2} - \langle S_A^z \rangle^2 - \langle S_B^z \rangle^2 - \langle S_A^- \rangle \langle S_A^+ \rangle - \langle S_B^- \rangle \langle S_B^+ \rangle \Big). \tag{21}$$

By minimizing $\langle H \rangle$, as given in equations (3) and (21), we find that the Bloch $\boldsymbol{k}$-state, $\gamma_{\boldsymbol{k}}$, diagonalizes an effective 4×4 Hamiltonian matrix, $H_{eff}(\boldsymbol{k})$, which can be expressed in the basis $(a_{\boldsymbol{k},\uparrow}, a_{\boldsymbol{k}+\boldsymbol{Q},\downarrow}, b_{\boldsymbol{k},\uparrow}, b_{\boldsymbol{k}+\boldsymbol{Q},\downarrow})$, as

$$H_{eff}(\boldsymbol{k}) = \begin{bmatrix} \mathcal{D}_A(\boldsymbol{k}) & \mathcal{C}^*(\boldsymbol{k}) \\ \mathcal{C}(\boldsymbol{k}) & \mathcal{D}_B(\boldsymbol{k}) \end{bmatrix} \tag{22}$$

where the 2×2 matrices D_α (with $\alpha = A, B$) and C are given by:

$$\mathcal{D}_\alpha(\boldsymbol{k}) = \begin{bmatrix} D(\boldsymbol{k}) - U\langle S^z \rangle - \mu & -U\langle S_\alpha^+ \rangle \\ -U\langle S_\alpha^- \rangle & D(\boldsymbol{k}+\boldsymbol{Q}) + U\langle S^z \rangle - \mu \end{bmatrix}, \tag{23}$$

and

$$\mathcal{C}(\boldsymbol{k}) = \begin{bmatrix} \phi(\boldsymbol{k}) & 0 \\ 0 & \phi(\boldsymbol{k}+\boldsymbol{Q}) \end{bmatrix}. \tag{24}$$

The mean field equations only determine the phase difference between $\langle S_A^+ \rangle$ and $\langle S_B^+ \rangle$, so we choose $\langle S_A^+ \rangle$ to be real. At each point in the weak ferromagnetic region of the phase diagram we have to choose the spiral wave vector $\boldsymbol{Q}$ that minimizes the ground state energy. This vector should lie along one of the high symmetry directions in the Brillouin Zone.

We first look for the most favorable wave vectors lying along the $\Gamma - X$ direction. For the same parameters as in figure 2, we find a spiral state with $\boldsymbol{Q} = \frac{1}{4}\boldsymbol{\Gamma X}$, $\langle S^z \rangle = 0.12$ and $\langle S_A^+ \rangle = 0.036$. We note that this spiraling state has a smaller z-component of the magnetization than that in the uniform phase. The angle between transverse magnetizations $\theta = 0.77\pi \approx 3\pi/4$. We find, however, that the energy difference between this spiral state and that with uniform magnetization is indeed very small, not exceeding $10^{-4}t$ per lattice site. This has been checked for several lattice sizes. We also note that the obtained spin transverse component is not negligible compared to $\langle S^z \rangle$. The most

favorable spiral wave vector depends slightly on interaction and density: at $U = 3.5$ and $n = 0.8$, for instance, $\boldsymbol{Q} = \frac{19}{80}\boldsymbol{\Gamma X}$ is the most favorable, with $\langle S^z \rangle = 0.089$, $\langle S^+_A \rangle = 0.046$ and $\theta = 0.73\pi$.

We now consider states with $\boldsymbol{Q} \propto \boldsymbol{\Gamma K}$. Overall, the energies of these spiral states are found to be lower than those of the states with $\mathbf{Q} \propto \mathbf{\Gamma X}$ considered above. For the same parameters as in figure 2, we find the optimum wave vector to be $\mathbf{Q} = \frac{3}{4}\mathbf{\Gamma K}$, where $\langle S^z \rangle$ vanishes and $\langle S^+_A \rangle = 0.24 = -\langle S^+_B \rangle$. The spin configuration is, therefore, planar and the two sub-lattices have opposite magnetizations. The energy (per lattice site) is 0.02 lower than that with uniform magnetization. An approximate representation of this state is shown in figure 5. The length of the most energetically favorable $\boldsymbol{Q}$ depends

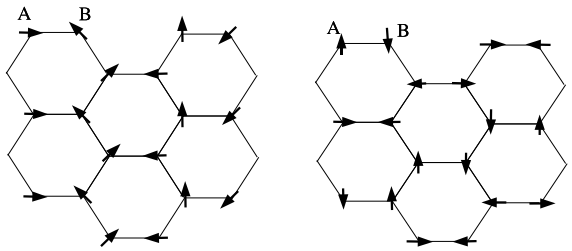

Figure 5. Representation of the spin transverse components $\langle S^+_{A,B} \rangle$ for the spiral states with: $\boldsymbol{Q} = (1/4)\boldsymbol{\Gamma X}$ (left); $\boldsymbol{Q} = (3/4)\boldsymbol{\Gamma K}$ (right). The latter configuration is purely planar and has the lowest energy for the same parameters as in figure 2.

significantly on U and n. If, for instance, $U = 3.5$ and $n = 0.8$, then $\mathbf{Q} = \frac{1}{2}\mathbf{\Gamma K}$ is the most favorable, with $\langle S^+_A \rangle = 0.18 = -\langle S^+_B \rangle$. The energy per lattice site of this state is 0.008 lower than that of the uniform state. In such a planar spin configuration, a small ferromagnetic alignment along z could still arise in the presence of a weak anisotropy or external magnetic field.

An anisotropic perturbation producing an easy axis (or a small magnetic field) need not exceed an energy of the order $10^{-2}t$ per lattice site in order to induce the uniform state, specially at the lower U values considered. It is still possible that the minimum energy spin structure of the system could be a superposition of spirals with different $\boldsymbol{Q}$ vectors, as has been found for the $n = 1$ Hubbard triangular lattice [18]. The search for such structures, as well as their sensitivity to disorder, is beyond the scope of this work, however. We also find that the spiral states are absent at smaller densities ($n < 0.6$). A schematic representations of our findings is shown in figure 6.

5. Disorder as possible mechanism to ferromagnetism

Ferromagnetic order induced by disorder in proton irradiated graphite was observed by Y. Kopelevich *et al.* [2]. The disorder induced by proton irradiation can be modeled by diagonal disorder, where the local energy of some sites is modified. The problem of

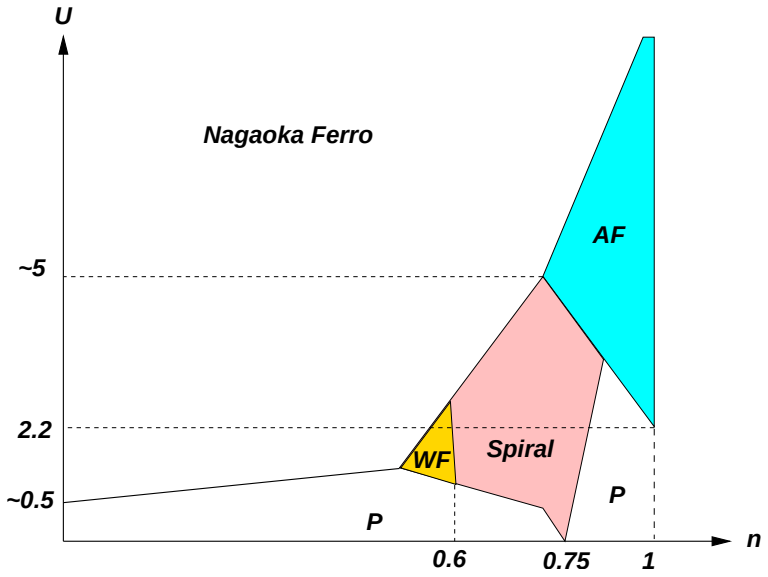

Figure 6. Schematic phase diagram of a honeycomb layer, with $t' \neq 0$, showing the paramagnetic (P), antiferromagnetic (AF), weak uniform ferromagnetic (WF) and spiral phases. The Nagaoka phase is a fully polarized ferromagnet. The exact position of the transition lines is not given, except at some special values marked in the axes. The results for $t' = 0$ are not qualitatively different.

treating disorder and Coulomb interaction together is a hard one in condensed matter physics [19]. Therefore we start by studying the effect of a finite density of uncorrelated impurities on the electron gas in the honeycomb lattice at half filling, where the low-energy electronic excitations can be described by massless Dirac fermions [15]. The effect of disorder on the properties of Dirac fermions leads to some unexpected results, and was discussed in the context of disordered superconductors by some authors [20, 21]. In our study, we compute the $T-$matrix using the massless Dirac fermion description.

The Matsubara Green's functions are determined via the equation-of-motion method. After the usual manipulations [22] we obtain the 2×2 Green's function matrix as

$$\boldsymbol{G}(\boldsymbol{p}, i\omega_n) = \boldsymbol{G}^0(\boldsymbol{p}, i\omega_n) + \boldsymbol{G}^0(\boldsymbol{p}, i\omega_n)\boldsymbol{T}(i\omega_n)\boldsymbol{G}^0(\boldsymbol{p}, i\omega_n)\,, \tag{25}$$

with the Matsubara $T-$matrix given by

$$\boldsymbol{T}(i\omega_n) = \frac{V}{N}[\mathbf{1} - \frac{V}{N}\bar{\boldsymbol{G}}^0(i\omega_n)]^{-1}\,, \tag{26}$$

where $\boldsymbol{G}^0(\boldsymbol{p}, i\omega_n)$ is the Green's function matrix with $V = 0$, and

$$\bar{\boldsymbol{G}}^0(i\omega_n) = \sum_{\boldsymbol{p}} \boldsymbol{G}^0(\boldsymbol{p}, i\omega_n)\,. \tag{27}$$

For a small density, n_{imp}, of scatterers (but finite in the thermodynamic limit), and after the position of the scatterers has been averaged over ensemble configurations, the Green's function matrix can be written as

$$\boldsymbol{G}(\boldsymbol{p}, i\omega_n) = [[\boldsymbol{G}^0(\boldsymbol{p}, i\omega_n)]^{-1} - \boldsymbol{\Sigma}(i\omega_n)]^{-1}\,, \tag{28}$$

where [22]

$$\mathbf{\Sigma}(i\omega_n) = V n_{imp}[\mathbf{1} - \frac{V}{N}\bar{\boldsymbol{G}}^0(i\omega_n)]^{-1}\,. \tag{29}$$

Once the Green's function (28) is known, one can proceed to include the effect of correlations into the problem. The electronic bound states are given by the poles of (26). There always is a bound state due to the impurity, below the energy band, independently of the value of V.

The existence of bound states allows for a possible mechanism to the disorder induced ferromagnetic behaviour in proton irradiated graphite. Graphite is usually modeled as a half-filled honeycomb plane, where electrons near the Fermi level have linear dispersion [15]. The sample irradiation produces the displacement of the carbon atoms from their original position. In this case, even if hydrogen atoms become bonded to some of the carbons, from the lattice point of view a dilution of lattice points is being induced. In this case, we should take the limit $V \to \infty$, even if n_{imp} is small. This effect leads to drastic change in the density of states $\rho(\omega)$, where a strong enhancement of $\rho(\omega)$ in the vicinity of $\omega = 0$ is obtained. Such an enhancement can be responsible for a large reduction of the critical U needed for ferromagnetism, as follows from the Stoner criterion. The effect of disorder on the density of states of Dirac fermions is shown in figure 7 for several values of n_{imp} and V. If V is negative there are bound states for the electrons below the bottom of the band. As V increases an enhancement of $\rho(\omega)$ in the vicinity of $\omega = 0$ starts to develop. We have, therefore, two possible routes toward

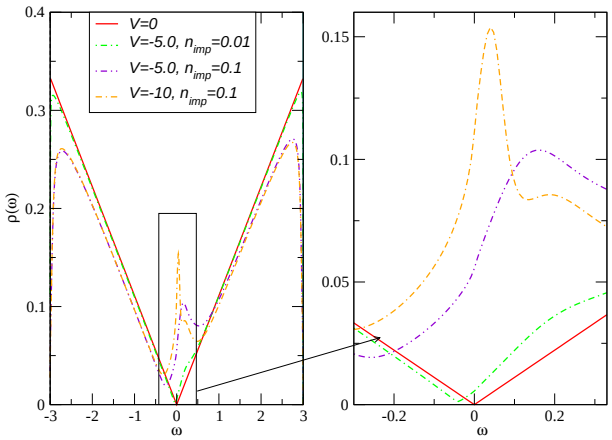

Figure 7. Density of states $\rho(\omega)$ for several impurity densities n_{imp} and V values, in a model of Dirac fermions. The left panel show ρ over the bandwidth. The right panel shows a zoom of the density of states presented in the left panel.

the appearance of magnetic order in graphite, namely bound states and enhancement of the density of states. This type of enhancement of $\rho(\omega)$ is characteristic of acoustic excitations, either fermionic (Dirac fermions) or bosonic (magnons)[23]. This very qualitative view has to be corroborated by more detailed calculations taking into account both disorder and Coulomb interaction. In particular, it is important to compute how

the critical lines from the paramagnetic to the magnetic phases change with the amount of disorder. These issues will be the subject of a future publication.

6. Conclusion

In conclusion, we have studied the spin collective excitations of the homogeneous weak ferromagnetic state in the honeycomb lattice and found an instability to spiral spin structures at electron densities above $n \approx 0.6$ Although our calculation is performed for a system with the same type of atoms it is simple to generalize it for honeycomb lattices with different type of atoms as in BNC hexagonal sheets [24]. However, the main differences will be: (i) the number of optical and acoustic branches increases; (ii) the different site energies due to different atoms will change the form of the spin wave bands. We have also suggested a possible mechanism for ferromagnetism in irradiated graphite: the appearance of bound states due to disorder and the enhancement of the density of states. If it becomes possible in the future to perform neutron scattering experiments on ferromagnetic graphite allotrope the results we present here may have direct experimental importance.

Acknowledgments

The authors would like to acknowledge A. H. Castro Neto for suggesting the $T-$matrix calculation and for many useful discussions on disordered systems. N.M.R.P is thankful to the Quantum Condensed Matter Visitor's Program at Boston University and Fundação para a Ciência e Tecnologia for a sabbatical grant partially supporting his sabbatical leave.

References

[1] P. W. Anderson, Science **235**, 1196 (1987)
[2] Y. Kopelevich, J. H. S. Torres, R. R. da Silva, F. Mrowka, H. Kempa and P. Esquinazi, Phys. Rev. Lett. **90**, 156402 (2003)
[3] L. Balents, M. P. A. Fisher and S. M. Girvin, Phys. Rev. B **65**, 224412 (2002)
[4] P. Esquinazi, A. Setzer, R. Höhne, C. Semmelhack, Y. Kopelevich, D. Spemann, T. Butz, B. Kohlstrunk and M. Lösche, Phys. Rev. B **66**, 24429 (2002); P. Esquinazi, D. Spemann, R. Höhne, A. Setzer, K. H. Han and T. Butz, Phys. Rev. Lett. **91**, 227201 (2003).
[5] K. Takada, H. Dakurai, E. Takayama-Muromachi, F. Izumi, R. A. Dilinian and T. Sasaki Nature **422**, 53 (2003)
[6] Y. Kopelevich, P. Esquinazi, J. H. S. Torres and S. Moehlecke, J. Low Temp. Phys. **119**, 691 (2000).
[7] T. Makarova, B. Sundqvist, R. Höhne, P. Esquinazi,Y. Kopelevich, P. Scharff, V. A. Davydov, L. S. Kashevarova and A. V. Rakhmanina, Nature **413**, 716 (2001)
[8] T. He and R. J. Cava, Phys. Rev. B **63**, 172403 (2001).
[9] K. S. Novoselov, A. K. Geim, S. V. Morozov, D. Jiang, Y. Zhang, S.V. Dubonos, I. V. Grigorieva and A. A. Firsov, Science **306**, 666 (2004).
[10] Y. Zhang, J. P. Small, W. V. Pontius and P. Kim cond-mat/410314.
[11] C. Berger, Z. Song, T. Li, X. Li, A. Y. Ogbazghi and R. Feng, cond-mat/410240.

[12] D. C. Mattis, Phys. Rev. **132**. 2521 (1964)
[13] H. Yamada and M. Shimizu, J. Phys. Soc. Japan **22**, 1404 (1967)
[14] N. M. R. Peres, M. A. N. Araújo and Daniel Bozi, Phys. Rev. B **70**, 195122 (2004)
[15] J. Gonzalez, F. Guinea and M. A. H. Vozmediano, Nucl. Phys. B **424**, 595 (1994) J. Gonzalez, F. Guinea, and M. A. H. Vozmediano, Phys. Rev. Lett. **77**, 3589 (1996).
[16] A. Singh and Z. Tesanovic, Phys. Rev. B **41**, 11457 (1990); **41**, 614 (1990)
[17] A. Auerbach, *Interacting Electrons and Quantum Magnetism*, (New York, Springer-Verlag, 1994) p.40.
[18] M. Fujita, T. Nakanishi and K. Machida, Phys. Rev. B **45**, 2190 (1992)
[19] W. Ziegler, D. Poilblanc, R. Preys, W. Hanke and D. J. Scalapino, Phys. Rev. B **53**, 8704 (1996).
[20] Patrick A. Lee, Phys. Rev. Lett. **71**, 1887 (1993).
[21] M.A.N. Araújo, Int. J. of Mod. Phys. B **15**, 409 (2001).
[22] S. Doniach and E. H. Sondheimer, *Green's functions for solid state physicists*, (London, Imperial College Press, 1988) chaps. 4 and 5.
[23] A. L. Chernyshev, Y. C. Chen and A. H. Castro Neto, Phys. Rev. Lett. **87**, 067209 (2001); *idem* Phys. Rev. B **65**, 104407 (2002).
[24] S. Okada and A. Oshiyama, Phys. Rev. Lett. **87**, 146803 (2001)